

FIMPs in a two-component dark matter model with $Z_2 \times Z_4$ symmetry

XINXIN QI^{1,*} and HAO SUN^{1,†}

¹*Institute of Theoretical Physics, School of Physics, Dalian University of Technology,
No.2 Linggong Road, Dalian, Liaoning, 116024, P.R.China*

We consider the FIMPs scenario in a two-component dark matter model with $Z_2 \times Z_4$ symmetry, where a singlet scalar S and a Majorana fermion χ are introduced as dark matter candidates. We also introduce another singlet scalar S_0 with a non-zero vacuum expectation value to the SM so that the fermion dark matter can obtain mass after spontaneous symmetry breaking. The model admits six free parameters in the decoupling limit: three masses and three dimensionless parameters. Depending on the mass hierarchies between dark matter particles with half of the new Higgs mass, the DM relic density will be determined by different channels, where χ and S production can be generated individually. We numerically study the relic density as a function of the model's free parameters and determine the regions consistent with the dark matter constraint for four possible cases. Our results show that this scenario is viable over a wide range of couplings and dark matter masses, where the coupling λ_{ds} can be as tiny as $\mathcal{O}(10^{-20})$ level. We stress that even for such tiny couplings, the new Higgs can still play a dominant role in determining dark matter production.

I. INTRODUCTION

The weakly interacting massive particle (WIMP) dark matter models are facing serious challenges since there are no signals found according to the current direct detection experiments for dark matter(DM)[1]. One possible solution for the null results is the feebly interacting massive particle (FIMP), where the observed dark matter relic density [1] is generated via the so-called "Freeze-in" mechanism[2]. "Freeze-in" assumes that dark matter particle interacts so feebly that it never reached thermally equilibrium in the early universe [3]. Moreover, due to the feeble interaction, it is difficult to search for FIMP in dark matter detectors.

On the other hand, there is no direct evidence showing that there is only one dark matter species, and multi-component dark matter models are also possible, which often involve two or more kinds of dark matter candidates. Discussion about multi-component dark matter models can be found in Refs.[4–21]. For these models, dark matter particles are often stabilized by additional discrete symmetry, where the visible sector and dark sector will carry different charges. Moreover, since one has two or more types of DM particles in the model, which constitute the observed DM relic density totally, each component can be generated via different production mechanisms. For the two-component dark matter models, there are two species of dark matter, and each component production can be generated individually, so we can have WIMPs, mixed WIMP-FIMP and FIMPs scenario.

In this work, we study the DM model proposed in Ref. [20, 22], but in light of the FIMPs scenario, we have two dark matter candidates in the model, a singlet scalar S and a Majorana fermion χ , which are stabilized by extra $Z_2 \times Z_4$ symmetry. Research about both singlet scalar and fermion as dark matter candidates can be found in [23–27]. The bare mass term of χ in the model is forbidden due to the $Z_2 \times Z_4$ symmetry, and we introduce another singlet scalar S_0 with a non-zero vacuum expectation value so that χ can acquire mass after spontaneous symmetry breaking. Note that one can assume S and S_0 carry the same Z_4 charge, and a Z_4 symmetry alone can be sufficient to guarantee the two stable dark matters. In this work, we consider a Z_2 symmetry to avoid the term SS_0 and simplify the scalar potential. For the FIMPs scenario, the production of S and χ can be generated individually, and conversion processes between dark matter particles are negligible due to the feeble interactions. Particularly, in the case of the decoupling limit, χ production is completely determined by the new Higgs and is independent of SM particles. We note that for the tiny mixing angle, SM particles can still contribute to χ relic density, but in this work, we fine-tune the value so that such a contribution can be negligible for simplicity. Remarkably, we have six parameters in the model -three masses and three dimensionless couplings. We show that, depending on the relation between the masses, contribution of different channels to the DM relic density are different, and we discuss the possible cases within this model. For each of them, we calculate DM relic density and determine the viable parameter space consistent with the DM constraint.

*Electronic address: qxx@dlut.edu.cn

†Electronic address: haosun@dlut.edu.cn

The paper is arranged as follows, in section. **II**, we give the two-component dark matter model with $Z_2 \times Z_4$ symmetry. In section. **III**, we briefly discuss the theoretical constraint on the model. In section. **IV**, we discuss the FIMPs scenario for the model and give the allowed parameter space, and finally we summarize in the last section of the paper.

II. MODEL DESCRIPTION

In this part, we consider a two-component dark matter model with $Z_2 \times Z_4$ symmetry by introducing two singlet scalars S and S_0 as well one Majorana fermion χ to the SM, where S and χ are dark matter candidates and S_0 owns non-zero vacuum expectation value (vev) v_0 , and the charges the particles in the model carrying are listed as follows:

Particle	$Z_2 \times Z_4$
SM	(1,1)
S	(-1,1)
S_0	(1,-1)
χ	(1,i)

TABLE I: The charges of the particles under $Z_2 \times Z_4$ symmetry.

The new additional Lagrangian is therefore given as follows:

$$\mathcal{L}_{new} \supset \frac{1}{2}M_1^2 S^2 + \frac{1}{4}\lambda_s S^4 - \frac{1}{2}\mu_0^2 S_0^2 + \frac{1}{4}\lambda_0 S_0^4 - \mu_H^2 |H|^2 + \lambda_H |H|^4 + \lambda_{dh} S^2 |H|^2 + \lambda_{ds} S^2 S_0^2 + \lambda_{sh} S_0^2 |H|^2 + y_{sf} S_0 \chi^T \chi \quad (1)$$

where H is the SM Higgs doublet. Under unitarity gauge, H and S_0 can be expressed with:

$$H = \begin{pmatrix} 0 \\ \frac{v+h}{\sqrt{2}} \end{pmatrix}, \quad S_0 = s_0 + v_0, \quad (2)$$

where $v = 246$ GeV corresponds to the electroweak symmetry breaking vev and v_0 is the vev of S_0 . After spontaneous symmetry breaking (SSB), the masses of S and χ can be given by:

$$m_S^2 = M_1^2 + 2\lambda_{ds}v_0^2 + \lambda_{dh}v^2, \quad m_\chi = y_{sf}v_0, \quad (3)$$

where $m_S(m_\chi)$ represents the mass of $S(\chi)$. On the other hand, we have the squared mass matrix of s_0 and h with:

$$\mathcal{M} = \begin{pmatrix} 2\lambda_0 v_0^2 & \lambda_{sh} v v_0 \\ \lambda_{sh} v v_0 & 2\lambda_H v^2 \end{pmatrix}. \quad (4)$$

The physical masses of the two Higgs states h_1, h_2 are then

$$\begin{aligned} m_1^2 &= \lambda_H v^2 + \lambda_0 v_0^2 - \sqrt{(\lambda_H v^2 - \lambda_0 v_0^2)^2 + (\lambda_{sh} v v_0)^2}, \\ m_2^2 &= \lambda_H v^2 + \lambda_0 v_0^2 + \sqrt{(\lambda_H v^2 - \lambda_0 v_0^2)^2 + (\lambda_{sh} v v_0)^2} \end{aligned} \quad (5)$$

The mass eigenstate (h_1, h_2) and the gauge eigenstate (h, s_0) can be related via

$$\begin{pmatrix} h_1 \\ h_2 \end{pmatrix} = \begin{pmatrix} \cos \theta & -\sin \theta \\ \sin \theta & \cos \theta \end{pmatrix} \begin{pmatrix} h \\ s_0 \end{pmatrix}. \quad (6)$$

where

$$\tan 2\theta = \frac{\lambda_{sh} v v_0}{\lambda_0 v_0^2 - \lambda_H v^2} \quad (7)$$

Furthermore, we can assume h_1 is the observed SM Higgs and h_2 is the new Higgs in our model. One can choose the masses of the Higgs particles m_1 and m_2 as the inputs so that the couplings of λ_H , λ_0 and λ_{sh} can be given by:

$$\begin{aligned}\lambda_H &= \frac{(m_1^2 + m_2^2) - \cos 2\theta(m_2^2 - m_1^2)}{4v^2}, \\ \lambda_0 &= \frac{(m_1^2 + m_2^2) + \cos 2\theta(m_2^2 - m_1^2)}{4v_0^2}, \\ \lambda_{sh} &= \frac{\sin 2\theta(m_2^2 - m_1^2)}{2vv_0}\end{aligned}\quad (8)$$

According to the current results, the mixing angle of the SM Higgs with other scalars is limited stringently arising from W boson mass correction [28] at NLO, the requirement of perturbativity and unitarity of the theory [29] as well as the LHC and LEP direct search [30, 31]. In this work, we consider the decoupling limit with $\sin \theta \rightarrow 0$ so that dark matter χ production is dominated by the new Higgs h_2 and the scalar dark matter S , where the relevant SM production is highly suppressed due to the tiny $\sin \theta$.

III. THEORETICAL CONSTRAINT

In this section, we discuss the theoretical constraints on the model from the point of perturbativity, perturbative unitarity and vacuum stability.

A. perturbativity

To ensure the perturbative model, the contribution from loop correction should be smaller than the tree level values, which put stringent constraints on the parameters with:

$$|2\lambda_{dh}| < 4\pi, |2\lambda_{ds}| < 4\pi, |y_{sf}| < \sqrt{4\pi}. \quad (9)$$

B. perturbative unitarity

The unitarity conditions come from the tree-level scalar-scalar scattering matrix which is dominated by the quartic contact interaction. The s-wave scattering amplitudes should lie under the perturbative unitarity limit, given the requirement the eigenvalues of the S-matrix \mathcal{M} must be less than the unitarity bound given by $|\text{Re}\mathcal{M}| < \frac{1}{2}$.

C. vacuum stability

To obtain a stable vacuum, the quartic couplings in the scalar potential should be constrained, In our model, the scalar potential quartic terms can be given with a symmetric 3×3 matrix as follows:

$$\mathcal{S} = \begin{pmatrix} \lambda_0 & \lambda_{sh} & \lambda_{ds} \\ \lambda_{sh} & \lambda_H & \lambda_{dh} \\ \lambda_{ds} & \lambda_{dh} & \frac{1}{4}\lambda_s \end{pmatrix}. \quad (10)$$

According to the copositive criterial, the vacuum stability demands the quartic couplings with:

$$\begin{aligned}\lambda_0, \lambda_H, \lambda_s &\geq 0, \lambda_{sh} + \sqrt{\lambda_0\lambda_H} \geq 0, \lambda_{ds} + \frac{1}{2}\sqrt{\lambda_0\lambda_s} \geq 0, \lambda_{dh} + \frac{1}{2}\sqrt{\lambda_H\lambda_s} \geq 0, \\ \frac{1}{2}\sqrt{\lambda_s}\lambda_{sh} + \lambda_{ds}\sqrt{\lambda_H} + \lambda_{dh}\sqrt{\lambda_0} + \sqrt{2(\lambda_{sh} + \sqrt{\lambda_0\lambda_H})(\lambda_{ds} + \frac{1}{2}\sqrt{\lambda_0\lambda_s})(\lambda_{dh} + \frac{1}{2}\sqrt{\lambda_H\lambda_s})} \\ &+ \frac{1}{2}\sqrt{\lambda_0\lambda_H\lambda_s} \geq 0.\end{aligned}\quad (11)$$

IV. FIMP DARK MATTER

We are interested in the case where the dark matter production is totally generated via the freeze-in mechanism. Concretely speaking, the number density of χ as well as S can be negligible at the early universe, and they never reached thermal equilibrium at the early universe due to the feeble interaction, which eventually determined the observed DM relic density nowadays with the decrease of the temperature.

A. Boltzmann equations

The current observed dark matter relic density given by the Planck collaboration is $\Omega_{DM}h^2 = 0.1198 \pm 0.0012$ [1], and we consider both χ as well as S production are generated with the “Freeze-in” mechanism, and S and χ will contribute to dark matter relic density totally. The Boltzmann equations for the abundance of S and χ are given as follows:

$$\frac{dY_S}{dx} = \frac{1}{3H} \frac{ds}{dx} [\langle \sigma v \rangle^{XX \rightarrow SS} \bar{Y}_X^2 + \langle \sigma v \rangle^{h_2 h_2 \rightarrow SS} \bar{Y}_{h_2}^2 + \theta(m_2 - 2m_S) \Gamma_{h_2 S} \bar{Y}_{h_2} + \theta(m_1 - 2m_S) \Gamma_{h_1 S} \bar{Y}_{h_1}], \quad (12)$$

$$\frac{dY_\chi}{dx} = \frac{1}{3H} \frac{ds}{dx} [\langle \sigma v \rangle^{h_2 h_2 \rightarrow \chi \chi} \bar{Y}_{h_2}^2 + \theta(m_2 - 2m_\chi) \Gamma_{h_2 \chi} \bar{Y}_{h_2}], \quad (13)$$

where $x = m_S/T$ with T being temperature, $\theta(x)$ is the Heaviside function, s denotes the entropy density, X represents SM particles. Y_S and Y_χ are abundance of S and χ defined by $Y_S \equiv n_S/s$ and $Y_\chi \equiv n_\chi/s$, where n_S and n_χ are number density of S and χ . \bar{Y}_{h_1} , \bar{Y}_{h_2} and \bar{Y}_χ are the abundance of h_1, h_2 and χ in thermal equilibrium, which are defined by:

$$\bar{Y}_{h_1} = \frac{45x^2 m_1^2}{2\pi^4 g_{*S} m_S^2} K_2\left(\frac{m_1}{m_S} x\right), \bar{Y}_{h_2} = \frac{45x^2 m_2^2}{2\pi^4 g_{*S} m_S^2} K_2\left(\frac{m_2}{m_S} x\right), \bar{Y}_\chi = \frac{45x^2 m_\chi^2}{2\pi^4 g_{*S} m_S^2} K_2\left(\frac{m_\chi}{m_S} x\right). \quad (14)$$

where $K_2(x)$ is the modified Bessel function of the second kind and g_{*S} is the number effective degrees of freedom. H is the Hubble expansion rate of the Universe, X denotes SM particles and $\langle \sigma v \rangle$ is the thermally averaged annihilation cross section. $\Gamma_{h_{1,2}S}$ and $\Gamma_{h_2\chi}$ represent the thermally averaged decay rate of $h_{1,2} \rightarrow SS$ and $h_2 \rightarrow \chi\chi$, which are defined by [32]:

$$\Gamma_{h_1 S} = \Gamma_{h_1 \rightarrow SS} \frac{K_1(m_1/T)}{K_2(m_1/T)}, \Gamma_{h_2 S} = \Gamma_{h_2 \rightarrow SS} \frac{K_1(m_2/T)}{K_2(m_2/T)}, \Gamma_{h_2 \chi} = \Gamma_{h_2 \rightarrow \chi\chi} \frac{K_1(m_2/T)}{K_2(m_2/T)}. \quad (15)$$

with

$$\Gamma_{h_1 \rightarrow SS} = \frac{\lambda_{dh}^2 v^2}{32\pi m_1} \sqrt{1 - \frac{4m_S^2}{m_1^2}}, \Gamma_{h_2 \rightarrow SS} = \frac{\lambda_{ds}^2 v_0^2}{32\pi m_2} \sqrt{1 - \frac{4m_S^2}{m_2^2}}, \Gamma_{h_2 \rightarrow \chi\chi} = \frac{y_{sf}^2 m_2}{4\pi} (1 - \frac{4m_\chi^2}{m_2^2})^{3/2},$$

where $K_1(x)$ is the modified Bessel function of the first kind.

B. Dependence on the parameters

In this work, we choose six free parameters as inputs in the model with:

$$m_\chi, y_{sf}, m_2, m_S, \lambda_{ds}, \lambda_{dh}. \quad (16)$$

Note that in the limit of $y_{sf} \rightarrow 0$, we come to the two singlet scalar DM model with S being FIMP, and in the limit of $\lambda_{ds} \rightarrow 0$ and $\lambda_{dh} \rightarrow 0$, the model can be simplified into the singlet fermion DM case with χ being FIMP. On the other hand, χ production is completely determined by dark sectors, and in the case of $m_\chi < m_2/2$, χ relic density is generated by the process of $h_2 \rightarrow \chi\chi$, and the decay width in Eq. 15 can be simplified far from the threshold:

$$\Gamma_{h_2 \rightarrow \chi\chi} \approx \frac{m_2 y_{sf}^2}{4\pi}, \quad (17)$$

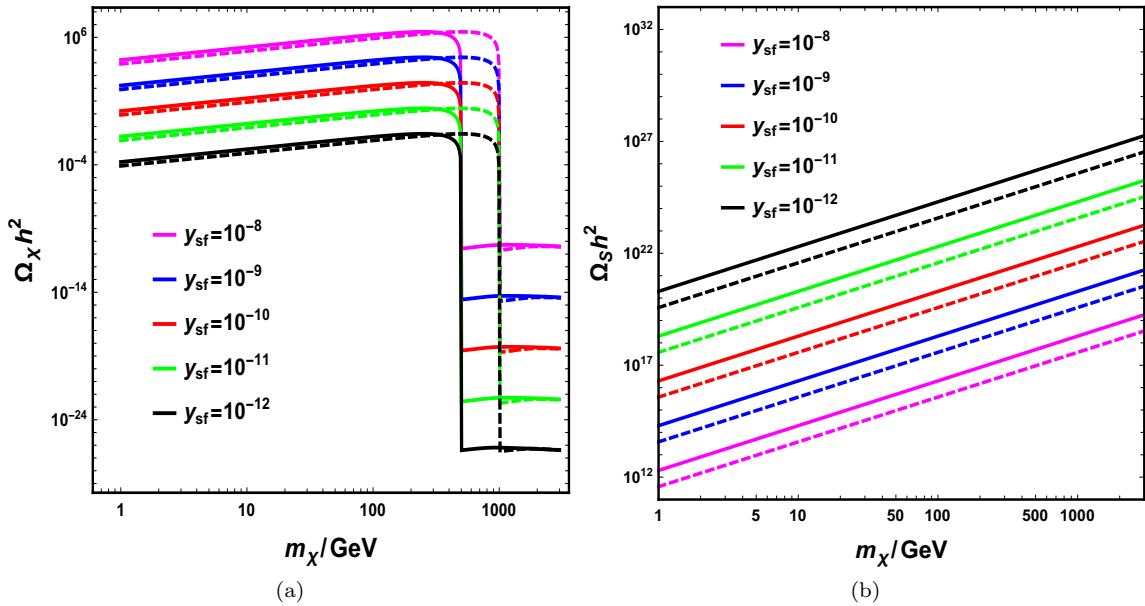


FIG. 1: Evolution of $\Omega_\chi h^2$ (left) and $\Omega_S h^2$ (right) with m_χ , where we have fixed $\lambda_{dh} = 10^{-10}$, $\lambda_{ds} = 10^{-10}$, $m_S = 400$ GeV. The different colored lines represent y_{sf} taking different values and the solid (dashed) lines correspond to the results of $m_2 = 1$ TeV ($m_2 = 2$ TeV) respectively.

The χ yield Y_χ can be computed by solving the Boltzmann equation Eq. 13, which can be simplified with:

$$sT \frac{dY_\chi}{dT} = -\frac{\gamma_{h_2 \rightarrow \chi\chi}(T)}{H(T)}, \quad (18)$$

where $H(T)$ is the expansion rate of the Universe at a given temperature and $\gamma_{h_2 \rightarrow \chi\chi}(T)$ is the thermal averaged FIMP production rate:

$$\gamma_{h_2 \rightarrow \chi\chi} = \frac{m_2^2 T}{2\pi^2} K_1(m_2/T) \Gamma_{h_2 \rightarrow \chi\chi}, \quad (19)$$

For high temperatures, $T > m_2$, we obtain [25]:

$$\frac{dY_\chi}{dT} \approx -10^7 \text{ GeV}^3 \left(\frac{m_2}{1 \text{ TeV}} \right)^2 \left(\frac{y_{sf}}{10^{-8}} \right)^2 T^{-4}. \quad (20)$$

We have that Y_χ always scales as the square of m_2 and of the Yukawa coupling y_{sf} when $T > m_2$. On the other hand, h_2 abundance becomes Boltzmann suppressed and the production of χ is no longer efficient. Therefore, we have:

$$Y_\chi(T \lesssim m_2) \approx 10^{-4} \left(\frac{1 \text{ TeV}}{m_2} \right) \left(\frac{y_{sf}}{10^{-8}} \right)^2, \quad (21)$$

The relic density of χ , $\Omega_\chi h^2$ is related to the asymptotic value of Y_χ at low temperatures by:

$$\Omega_\chi h^2 = 2.744 \times 10^8 \frac{m_\chi}{\text{GeV}} Y_\chi(T_0), \quad (22)$$

where $T_0 = 2.752$ K is the present day cosmic microwave background (CMB) temperature. For χ production obtained with the Freeze-in mechanism, χ relic density can be estimated as [25]:

$$\Omega_\chi h^2 \approx 0.3 \left(\frac{m_\chi}{0.1 \text{ GeV}} \right) \left(\frac{y_{sf}}{10^{-10}} \right)^2, \quad (23)$$

where we used Eq. 21 and Eq. 22. In the case of $m_2 = 1$ TeV, $m_\chi = 1$ GeV and DM relic density is totally composed by χ , one can estimate that y_{sf} should be smaller than $\mathcal{O}(10^{-11})$. When m_χ is larger than $m_2/2$, χ production is

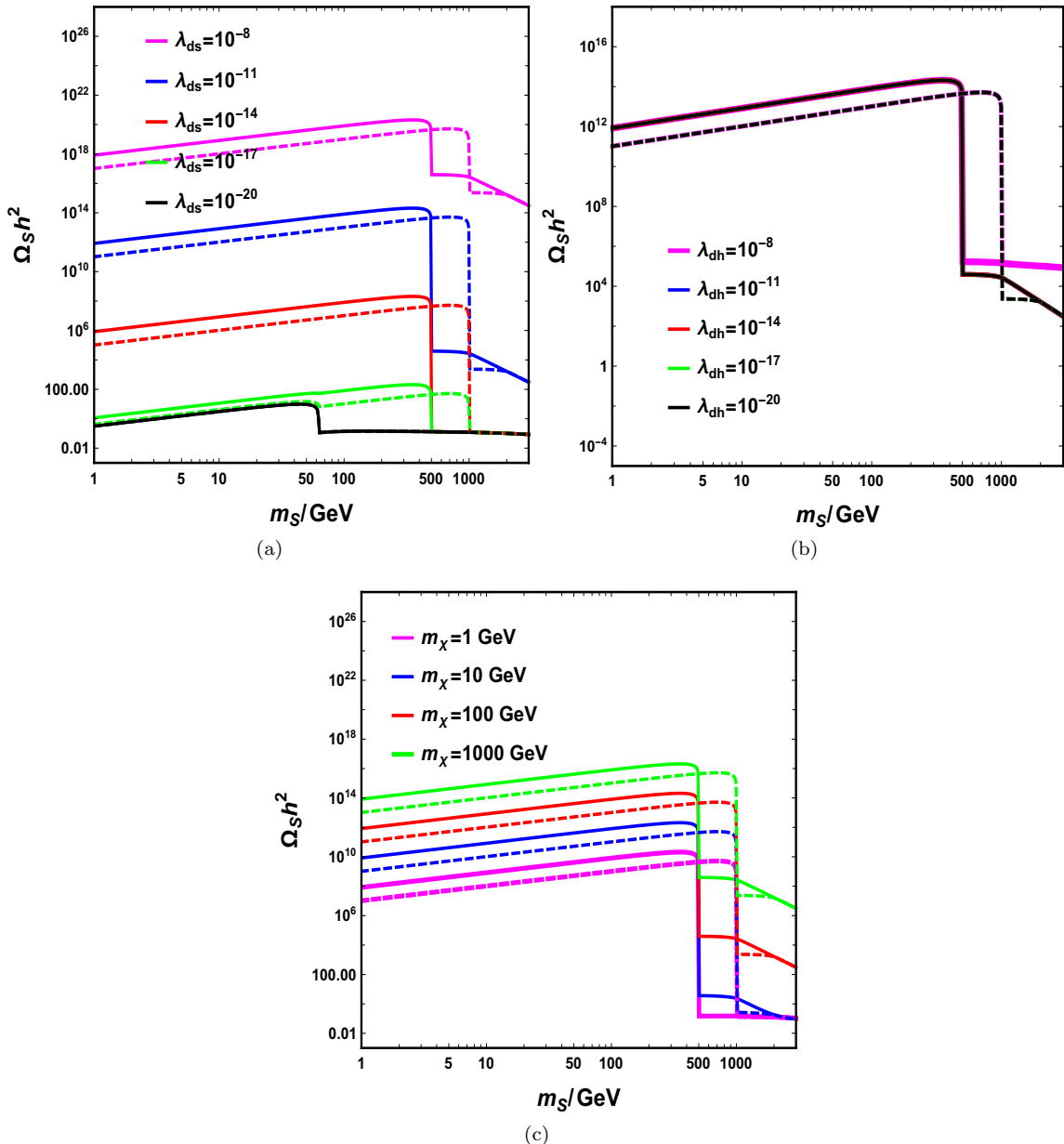


FIG. 2: Evolution of $\Omega_S h^2$ with m_S , where we fixed $y_{sf} = 10^{-11}$. In Fig. 2(a), we set $\lambda_{dh} = 10^{-11}$ and $m_\chi = 100$ GeV, while lines with different colors represent λ_{ds} taking different values. The solid lines are results of $m_2 = 1$ TeV while the dashed lines are $m_2 = 2$ TeV. In Fig. 2(b), we fix $\lambda_{ds} = 10^{-11}$ and vary λ_{dh} ranging from $[10^{-20}, 10^{-8}]$ while other parameter are same with the Fig. 2(a), and the lines with different colors correspond to λ_{dh} taking different values. In Fig. 2(c), we fix $\lambda_{ds} = 10^{-11}$ and vary m_χ ranging from $[1\text{GeV}, 1000\text{GeV}]$ while other parameter are same with the Fig. 2(a), and the lines with different colors correspond to m_χ taking different values.

generated via the $2 \rightarrow 2$ processes and the Yukawa coupling y_{sf} can not necessarily be so small. We stress that the results shown in this and all the following figures were obtained with Micromegas and not with the analytical expressions obtained in the text, which serve instead as a check and illustrate the functional dependence on the different parameters.

In this work, we focus on the case of both S and χ being FIMPs, while the production of S and χ can be generated individually. Relic density of χ is exactly determined by the parameters y_{sf}, m_χ and m_2 , while S is given by $m_S, m_2, \lambda_{ds}, \lambda_{dh}$ and m_χ/y_{sf} . Note that although χ will not make a difference in the production of S , the vev $v_0 = m_\chi/y_{sf}$ is related to the processes of $h_2 h_2 \rightarrow SS$ as well as $h_2 \rightarrow SS$ so that relic density of S is determined by the five parameters.

In Fig. 1, we show the evolution of $\Omega_\chi h^2$ (left) and $\Omega_S h^2$ (right) with m_χ , where we have fixed $\lambda_{dh} = 10^{-10}$, $\lambda_{ds} = 10^{-10}$, $m_S = 400$ GeV. The different colored lines represent y_{sf} taking different values, and the solid (dashed) lines correspond to the results of $m_2 = 1$ TeV ($m_2 = 2$ TeV), respectively. According to Fig. 1(a), in the case of $m_2 = 1$ TeV, when $m_\chi < 500$ GeV, χ production is mainly determined by the decay process of $h_2 \rightarrow \chi\chi$, and we will have a larger $\Omega_\chi h^2$ for a larger y_{sf} due to the stronger decay rate. On the other hand, for the fixed y_{sf} , $\Omega_\chi h^2$ will increase with the increase of m_χ as we can in Fig. 1(a). As $m_\chi > m_2/2$, χ production is obtained via the process of $h_2 h_2 \rightarrow \chi\chi$, where the curve drops sharply for the fixed y_{sf} . For a heavier m_2 with $m_2 = 2$ TeV, we have similar behaviors of the curves, but the lines drop sharply at about $m_\chi \approx 1$ TeV. In Fig. 1(b), we show the evolution of $\Omega_S h^2$ with m_χ . As we mentioned above, although S and χ production can be generated individually, S relic density is related to m_χ/y_{sf} , and for the fixed y_{sf} , $\Omega_S h^2$ increase with the increase of m_χ while for the fixed m_χ , a larger y_{sf} will contribute to a smaller $\Omega_S h^2$ instead. On the other hand, S production is mainly determined by the process of $XX \rightarrow SS$ as well as $h_2 \rightarrow SS$, where X represents SM particles, and for the heavier m_2 with $m_2 = 2$ TeV, we have small decay width and the dashed lines lie below the respective solid lines as we can see in Fig. 1(b).

As we mentioned above, parameters related to $\Omega_S h^2$ are λ_{ds} , λ_{dh} , m_S as well as m_χ/y_{sf} . For m_S belonging to different mass regions, S production can be generated via different processes. Concretely speaking, as $m_S < m_1/2$, the decay processes $h_{1,2} \rightarrow SS$ contribute to S production. In the case of $m_1/2 < m_S < m_2/2$, S production is mainly determined by $XX \rightarrow SS$ and $h_2 \rightarrow SS$ with X being SM particles. For $m_S > m_2/2$, S production is obtained via the $2 \rightarrow 2$ processes with $XX \rightarrow SS$ and $h_2 h_2 \rightarrow SS$. We give the evolution of $\Omega_S h^2$ with m_S in Fig. 2, where we fixed $y_{sf} = 10^{-11}$. In Fig. 2(a), we set $\lambda_{dh} = 10^{-11}$ and $m_\chi = 100$ GeV, while lines with different colors represent λ_{ds} taking different values. The solid lines are results of $m_2 = 1$ TeV, while the dashed lines are $m_2 = 2$ TeV. For $\lambda_{ds} = 10^{-8}$, 10^{-11} and 10^{-14} , processes involve h_2 play a dominant role in determining S relic density and the curves sharply drop as m_S approximate to $m_2/2$, where $h_2 \rightarrow SS$ is dominant in determining S production in the case of $m_S < h_2/2$ and $h_2 h_2 \rightarrow SS$ becomes efficient when $m_S > m_2/2$. On the other hand, when $m_S > 1$ TeV, $\Omega_S h^2$ decreases with the increase of m_S since the process $h_2 h_2 \rightarrow SS$ is kinetically suppressed for $m_2 < m_S$. We have similar conclusion of $m_2 = 2$ TeV, but the curves drops at about $m_S = 1$ TeV ($m_S \approx m_2/2$) and $m_S = 2$ TeV ($m_S \approx m_2$). For $\lambda_{ds} = 10^{-17}$, both SM particles and h_2 will contribute to S production, where $\Omega_S h^2$ is much smaller compared with the former cases. When $m_S < m_1/2$, $\Omega_S h^2$ increases with the increase of m_S , and when m_S approximate to $m_1/2$, the curve has a slight drop, which corresponds to the case that decay of $h_1 \rightarrow SS$ is forbidden and $XX \rightarrow SS$ becomes efficient to S production, and such drop can be more obvious in the case of $m_2 = 2$ TeV since contribution of h_2 to S production is more suppressed for the heavier m_2 . Similarly, we can also find a sharp drop at about $m_S \approx m_2/2$, where $h_2 \rightarrow SS$ is closed, and $h_2 h_2 \rightarrow SS$ is opened and contributes to S production along with $XX \rightarrow SS$. Particularly, when $m_S > m_2$, the curve will not drop as in the former cases since the contribution of $h_2 h_2 \rightarrow SS$ is less efficient for S production for the tiny λ_{ds} . For the case of $\lambda_{ds} = 10^{-20}$, SM particles will play a dominant role in determining DM relic density, and the black lines almost coincide for $m_2 = 1$ TeV and $m_2 = 2$ TeV. Unlike with the former cases, the black curves will only drop sharply at about $m_S \approx m_1/2$ since processes related to h_2 make little difference in DM relic density for the case of $\lambda_{ds} = 10^{-20}$.

In Fig. 2(b), we fix $\lambda_{ds} = 10^{-11}$ and vary λ_{dh} ranging from $[10^{-20}, 10^{-8}]$ while other parameter are same with the Fig. 2(a), and the lines with different colors correspond to λ_{dh} taking different values. As we mentioned above, for the large λ_{ds} , processes related to h_2 plays a dominant role in determining S production, and the solid (dashed) lines are almost coincide with each other with $m_2 = 1$ TeV ($m_2 = 2$ TeV), where the value of λ_{dh} almost make little difference in $\Omega_S h^2$. However, for $\lambda_{dh} = 10^{-8}$ and $m_2 = 1$ TeV, SM particles can play an important role in determining S relic density and the curve will not drop sharply for the larger m_S like other solid curves in the case of $m_S > 1$ TeV with the process of $h_2 h_2 \rightarrow SS$ being less efficient. According to Fig. 2(c), we fix $\lambda_{ds} = 10^{-11}$ and vary m_χ ranging from $[1\text{GeV}, 1000\text{GeV}]$ while other parameter are same with the Fig. 2(a), and the lines with different colors correspond to m_χ taking different values. Note that S and χ production are generated individually via the "Freeze-in" mechanism and for the fixed y_{sf} , varying of m_χ will contribute to the change of v_0 , defined by m_χ/y_{sf} , which is related to the cross section of $h_2 h_2 \rightarrow SS$ and $h_2 \rightarrow SS$. According to Fig. 2(c), a larger $m_\chi(v_0)$ will induce a larger cross section of $h_2 \rightarrow SS$ and $h_2 h_2 \rightarrow SS$ so that we have a larger $\Omega_S h^2$. For $m_\chi = 1$ GeV, the process $h_2 h_2 \rightarrow SS$ becomes less efficient as $m_\chi > 500$ GeV, and $\Omega_S h^2$ almost unchanged with the increase of m_S . On the other hand, for $m_2 = 2$ TeV, the dashed lines always lie below the solid lines for the fixed m_χ when $m_S < 500$ GeV due to the smaller decay width. For $500\text{GeV} < m_S < 1$ TeV, the dashed lines are above the solid ones where S production is generated via the decay process $h_2 \rightarrow SS$ for the former case and annihilation process $h_2 h_2 \rightarrow SS$ for the latter case. Furthermore, as $1\text{TeV} < m_S < 2$ TeV, the dashed lines lie below the solid ones for the smaller cross section of $h_2 h_2 \rightarrow SS$. When $m_S > 2$ TeV, the process $h_2 h_2 \rightarrow SS$ becomes less efficient and SM particles play a dominant role in determining S relic density so that the dashed lines and solid lines almost coincide with each other for the fixed m_χ .

C. Discussion

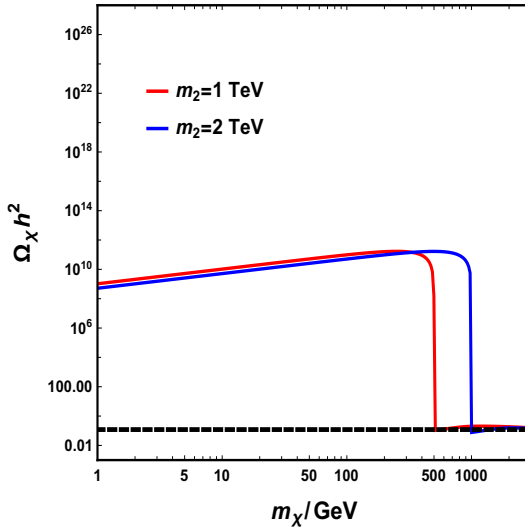


FIG. 3: Evolution of $\Omega_\chi h^2$ with m_χ by setting $y_{sf} = 2.5 \times 10^{-6}$, where the black dashed line corresponds to the observed DM relic density.

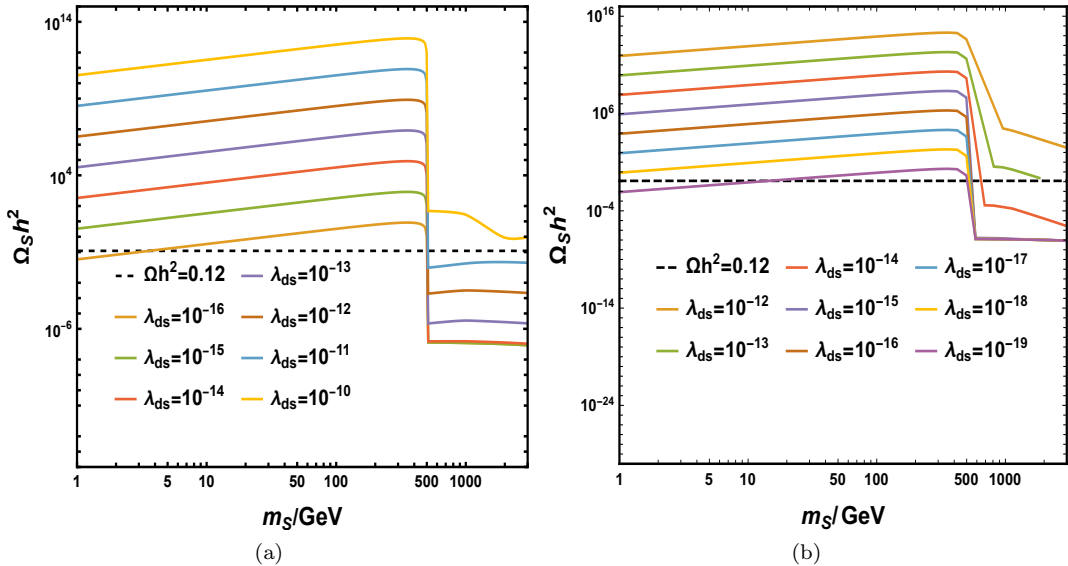
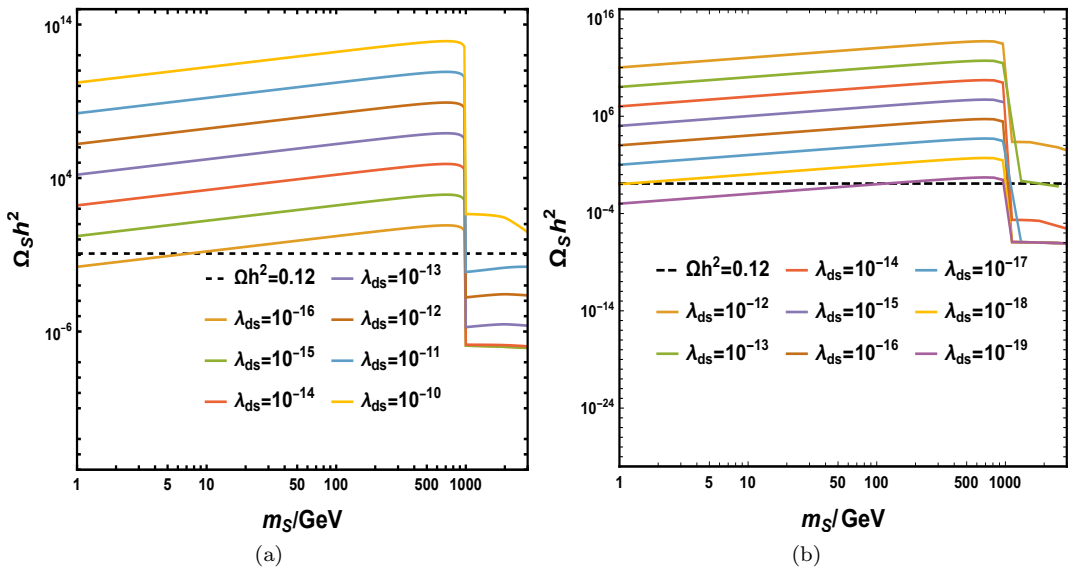


FIG. 4: Evolution of $\Omega_S h^2$ with m_S by fixing $\lambda_{dh} = 10^{-14}$ and $m_2 = 1$ TeV, where in the left figure we set $y_{sf} = 2.5 \times 10^{-6}$ as well as $m_\chi = 501$ GeV and we fix $y_{sf} = 10^{-11}$ and $m_\chi = 1$ GeV in the right figure. The black dashed lines represent the current observed DM relic density of $\Omega h^2 = 0.12$ and other colored lines correspond to the results of λ_{ds} taking different values.

As we mentioned above, one feature of our model for the FIMP scenario is that χ and S production are generated individually but the parameters y_{sf} and m_χ related to $\Omega_\chi h^2$ can also make difference in $\Omega_S h^2$ via the process $h_2 h_2 \rightarrow SS$, where $v_0(m_\chi/y_{sf})$ will be much large due to the tiny y_{sf} so that the allowed λ_{ds} will be much smaller compared with the traditional FIMP models under DM relic density constraint, and we will focus on the value of y_{sf} and λ_{ds} in the following discussion. According to the dependence of DM relic density on the couplings, $\Omega_S h^2$ will increase with the increase of $\lambda_{ds}, \lambda_{dh}$ as well as m_χ/y_{sf} . In the case of $m_\chi < m_2/2$, one can roughly estimate the upper bound of y_{sf} is about $y_{sf} < 10^{-11}$ for $m_2 = 1$ TeV under DM relic density constraint and such a tiny value will demand a much tiny λ_{ds} to obtain the correct $\Omega_S h^2$. For $m_\chi > m_2/2$, χ production is determined by the process $h_2 h_2 \rightarrow \chi\chi$, and the value of y_{sf} can not be necessarily so tiny according to Fig. 1. However, the large y_{sf} can contribute to S

FIG. 5: Same as Fig. 4 but $m_2 = 2$ TeV.

production over-abundance and the parameter space will be more constrained for $m_\chi > m_2/2$. To estimate the viable parameter space of the model under DM relic density, we first consider the possible upper bound of y_{sf} in the case of $m_\chi > m_2/2$. In Fig. 3, we show the evolution of $\Omega_\chi h^2$ with m_χ by setting $y_{sf} = 2.5 \times 10^{-6}$, where the black dashed line corresponds to the observed DM relic density. Note that $\Omega_\chi h^2$ is only related to y_{sf} , m_2 and m_χ and here we fixed $m_S = 400$ GeV, $\lambda_{ds} = 10^{-10}$ and $\lambda_{dh} = 10^{-10}$ for simplicity, where the red (blue) line represents the results of $m_2 = 1$ TeV ($m_2 = 2$ TeV). According to Fig. 3, the red line is almost coincide with the dashed black line when $m_\chi > 500$ GeV, and one can roughly estimate the upper bound of y_{sf} is about 2.5×10^{-6} for $m_2 = 1$ TeV, and we have similar conclusion for $m_2 = 2$ TeV. Note that the upper bound of y_{sf} corresponds to the case that S production can be negligible under DM relic density. On the other hand, the exact value for the upper bound of y_{sf} can be calculated analytically, but here we give a rough estimate and this has little impact on our final conclusion.

Moreover, we determine the upper bound of λ_{ds} for the fixed y_{sf} . We show the evolution of $\Omega_S h^2$ with m_S in Fig. 4 by fixing $\lambda_{dh} = 10^{-14}$ and $m_2 = 1$ TeV, where in the left figure we set $y_{sf} = 2.5 \times 10^{-6}$ as well as $m_\chi = 501$ GeV and we fix $y_{sf} = 10^{-11}$ and $m_\chi = 1$ GeV in the right figure. The black dashed lines represent the current observed DM relic density of $\Omega h^2 = 0.12$, and other colored lines correspond to the results of λ_{ds} taking different values. Here we have set the values of m_χ and λ_{dh} as small as possible while y_{sf} as large as possible according to Fig. 1 and Fig. 3, and we can therefore estimate the upper bound of λ_{ds} roughly under DM relic density constraint. According to Fig. 4(a), for $m_S < 500$ GeV, the allowed λ_{ds} should be smaller than 10^{-15} to obtain the correct DM relic density, while for $m_S > m_2/2$, since the dominant process related to S production is $h_2 h_2 \rightarrow SS$ for the tiny λ_{dh} and the allowed λ_{ds} value can be much larger, and we have $\lambda_{ds} < 10^{-10}$. In the case of $m_\chi = 1$ GeV, we have similar conclusion but the allowed λ_{ds} is much smaller than $\lambda_{ds} < 10^{-18}$ for $m_S < 500$ GeV. On other hand, as $m_S > 500$ GeV, the allowed value for λ_{ds} should be smaller than 10^{-12} . In Fig. 5, we keep other parameters unchanged but set $m_2 = 2$ TeV as in Fig. 4. We have similar conclusion for the upper bound of λ_{ds} and λ_{ds} should be smaller than 10^{-17} for $m_S < m_2/2$ according to Fig. 5(b). As for the value of λ_{dh} , we have the following comment. when λ_{ds} is tiny and contribution of h_2 to S relic density can be negligible so that S production is mainly related to SM Higgs (h_1). The viable parameter space for $\lambda_{ds} - m_S$ will be consistent with the singlet scalar DM model, where λ_{dh} is at $10^{-12} - 10^{-11}$ level for the correct DM relic density in the absence of χ in our model. For simplicity, in the following discussion to estimate the allowed parameter space, we make a random scan for λ_{dh} within $[10^{-14}, 10^{-11}]$, where the lower bound corresponds to the case that SM particles make little difference in S production.

$500\text{GeV} < m_\chi < 3\text{ TeV}$ and $m_S < 500$ GeV.

As we mentioned above, the allowed for the couplings are different for different mass hierarchies, and to obtain the viable parameter space of the model under DM relic density constraint, we consider 4 different cases with i) $m_\chi < m_2/2, m_S < m_2/2$, ii) $m_\chi < m_2/2, m_S > m_2/2$, iii) $m_\chi > m_2/2, m_S < m_2/2$ and iv) $m_\chi > m_2/2, m_S > m_2/2$. For simplicity, we fix $m_2 = 1$ TeV and make a random scan for the couplings with

$$\lambda_{dh} \subseteq [10^{-14}, 10^{-11}], y_{sf} \subseteq [10^{-14}, 2.5 \times 10^{-6}], \lambda_{ds} \subseteq [10^{-24}, 10^{-10}]. \quad (24)$$

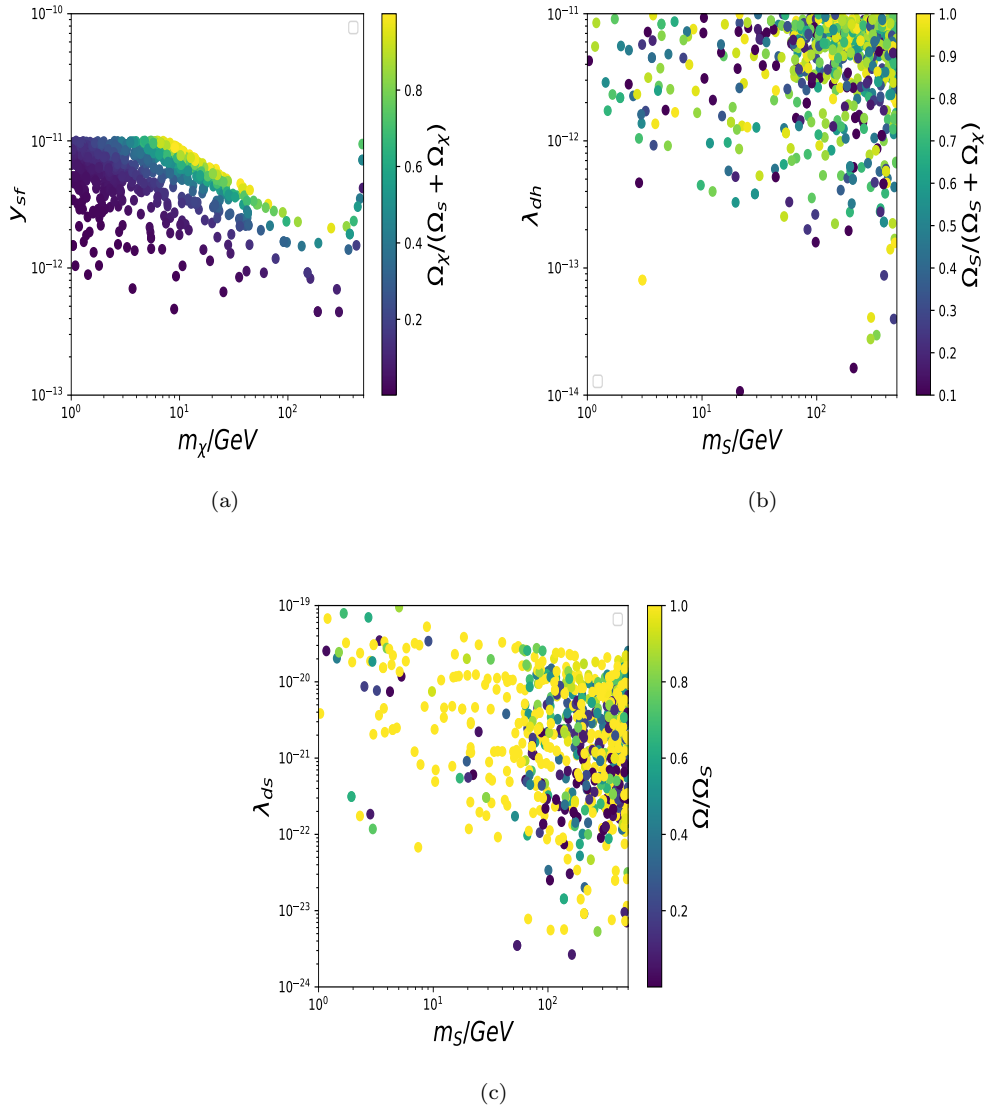


FIG. 6: Results of $m_\chi < 500$ GeV and $m_S < 500$ GeV. (a) shows the viable parameter space of $m_\chi - y_{sf}$ under DM relic density constraint, where points with different colors represent the fraction of χ defined by $\Omega_\chi/(\Omega_\chi + \Omega_S)$. (b) shows the viable parameter space of $m_S - \lambda_{dh}$, where points with different colors represent the fraction of S defined by $\Omega_S/(\Omega_\chi + \Omega_S)$. (c) shows the viable parameter space of $m_S - \lambda_{ds}$, where points with different colors represent the contribution of h_2 to S relic density defined by $\Omega/(\Omega_S)$.

In Fig. 6, we give the viable parameter space for $m_\chi < 500$ GeV and $m_S < 500$ GeV, where χ production is determined by the process $h_2 \rightarrow \chi\chi$ and S production is generated via $h_2 \rightarrow SS$ as well as $XX \rightarrow SS$ with X being SM particles. According to Fig. 6(a), we show the viable parameter space of $m_\chi - y_{sf}$ under DM relic density constraint, where points with different colors represent the fraction of χ in DM defined by $\Omega_\chi/(\Omega_\chi + \Omega_S)$ with Ω_χ being χ relic abundance and Ω_S being S relic abundance. The allowed value for y_{sf} is about $(3 \times 10^{-13}, 10^{-11}]$ while m_χ can take value among $[1 \text{ GeV}, 500 \text{ GeV}]$. As m_χ is small, $\Gamma_{h_2} \rightarrow \chi\chi$ is approximately equal to $\frac{y_{sf} m_2}{4\pi}$, and the fraction of χ is always sub-dominant among the total DM relic density regardless of y_{sf} . For $m_\chi \geq 7 \text{ GeV}$, DM can be mostly constituted by the χ production for a large y_{sf} as we can see in Fig. 6(a), where the larger y_{sf} will always contribute to a larger fraction of χ . With the increase of m_χ , the upper bound of y_{sf} will decrease under the DM relic density constraint. However, when m_χ is larger than about 300 GeV, the upper bound of the allowed y_{sf} value will increase as m_χ increases to obtain the correct relic density due to the phase-space suppression for the heavy χ . In Fig. 6(b), we give the result of $m_S - \lambda_{dh}$, where points with different colors correspond to the fraction of S

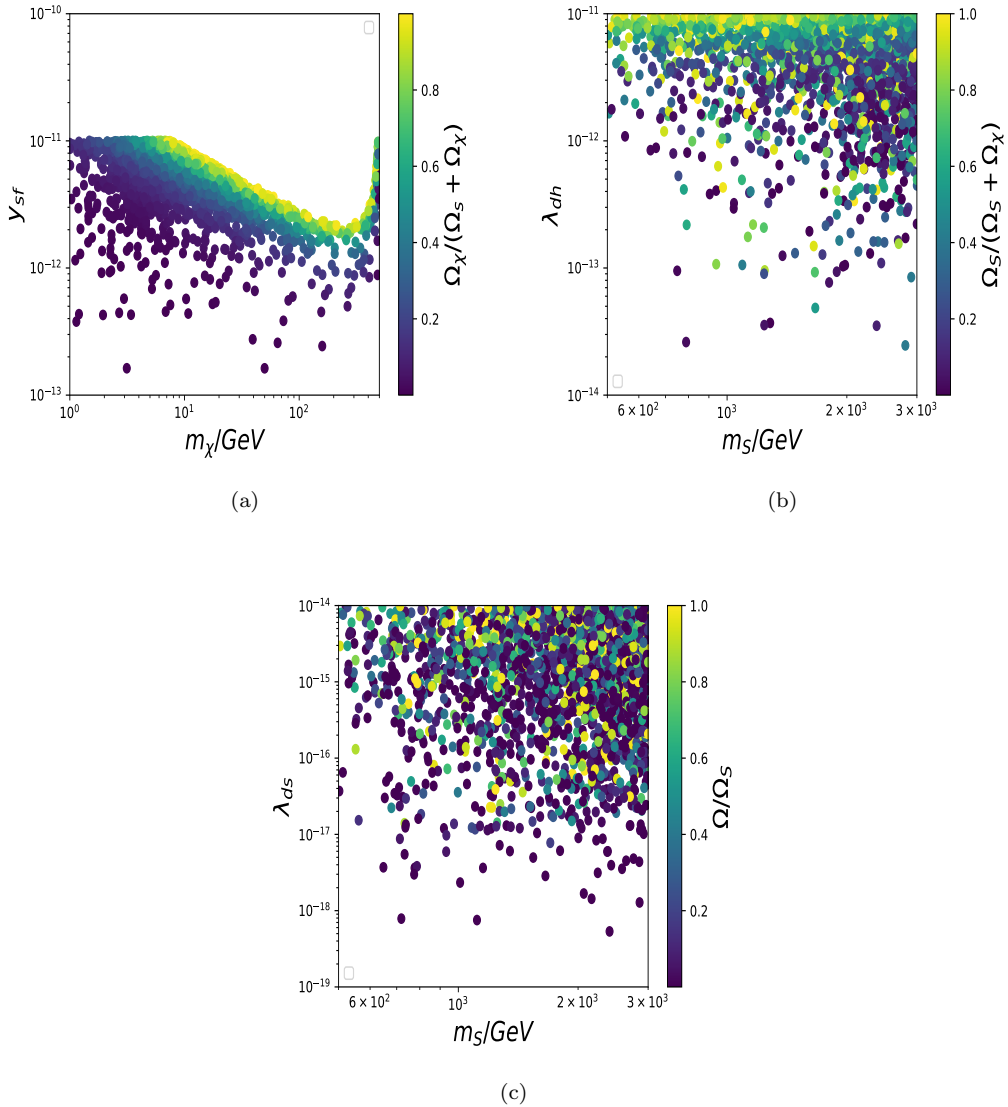


FIG. 7: Same as Fig. 6 but $m_\chi < 500$ GeV and $500\text{GeV} < m_S < 3000$ GeV.

defined by $\Omega_S/(\Omega_S + \Omega_\chi)$. m_S can take a value among the whole chosen mass region of [1 GeV, 500 GeV], and most of the points lie in the upper right of the plane, indicating that a lighter S always demands a larger λ_{dh} to obtain the correct DM relic density. With the increase of m_S , the allowed value for λ_{dh} is more flexible according to Fig. 6(b). On the other hand, for the small λ_{dh} such as $\lambda_{dh} = 8 \times 10^{-14}$, the fraction of S can be dominant where processes related to h_2 play an important role in determining S production. In Fig. 6(c), we show the viable parameter space of $m_S - \lambda_{ds}$, and points with different colors represent the contribution of h_2 to S relic density defined by Ω/Ω_S , where Ω is determined by the process of $h_2 \rightarrow SS$ for $m_S < 500$ GeV. As we mentioned above, the allowed λ_{ds} value should be much small to obtain the correct DM relic density compared with the traditional FIMP models, and here λ_{ds} is constrained within $(2 \times 10^{-24}, 10^{-19}]$ according to Fig. 6(c). The points almost lie in the upper-right region of the plane, indicating that a light S always demands a large λ_{ds} under DM relic density constraint. However, as $m_S > 100$ GeV, the upper bound of λ_{ds} is limited with $\lambda_{ds} < 2 \times 10^{-20}$. On the other hand, most of the points correspond to $\Omega/\Omega_S \approx 1$, which means that the process of $h_2 \rightarrow SS$ plays a dominant role in determining S relic density.

According to Fig. 7, we give the results of $m_\chi < 500$ GeV and $500\text{GeV} < m_S < 3000$ GeV. In this case, χ production is mainly determined by the process of $h_2 \rightarrow \chi\chi$, and we therefore have a similar conclusion for the viable parameter space of $m_\chi - y_{sf}$ as we can see in Fig. 7(a) with case i. In Fig. 7(b), we show the allowed parameter space of $m_S - \lambda_{dh}$, where m_S can take value ranging from [600GeV, 3TeV] and λ_{dh} is constrained within $[2 \times 10^{-14}, 10^{-11}]$. For the large

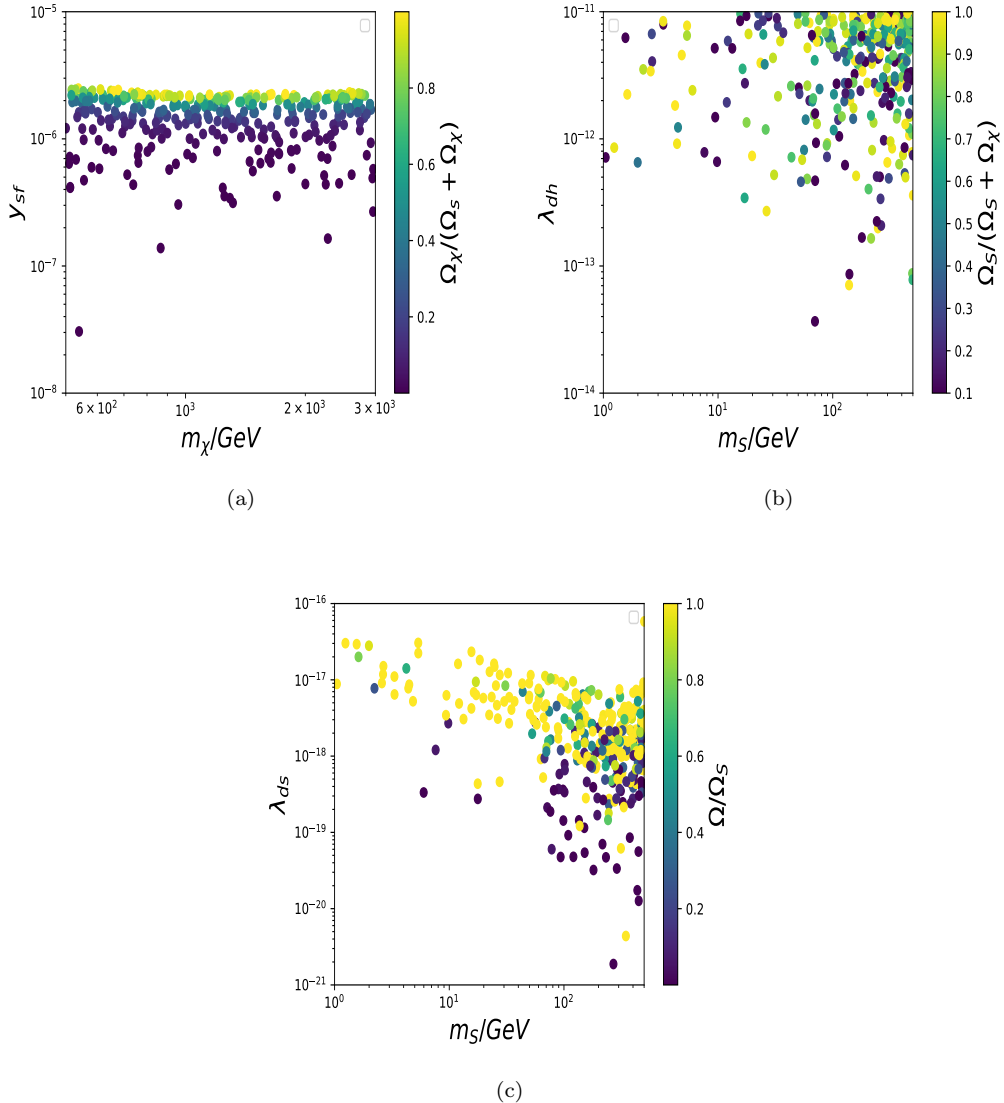


FIG. 8: Same as Fig. 6 but $500\text{GeV} < m_\chi < 3\text{ TeV}$ and $m_S < 500\text{ GeV}$.

λ_{dh} , the fraction of S is dominant in DM relic density, which means that processes related to SM particles play an important role in determining S production for the large λ_{dh} . In Fig. 7(c), we show the viable parameter space of $m_S - \lambda_{ds}$, and points with different colors correspond to the contribution of h_2 to S production, which is determined by the process of $h_2h_2 \rightarrow SS$ in this case. According to Fig. 7(c), λ_{ds} is limited within $(4 \times 10^{-19}, 10^{-14}]$, and most of the points correspond to the fraction Ω/Ω_S smaller than 0.4 indicating that contribution of h_2 to S production is sub-dominant compared with the SM particles. On the other hand, for $\lambda_{ds} > 2 \times 10^{-17}$, the fraction Ω/Ω_S can be approximate to 1 by choosing proper λ_{dh} under DM relic density constraint.

In Fig. 8, we give the result of $500\text{GeV} < m_\chi < 3\text{ TeV}$ and $m_S < 500\text{ GeV}$, where χ production is determined by the process $h_2h_2 \rightarrow \chi\chi$. According to Fig. 8, we show the viable parameter space of $m_\chi - y_{sf}$, where points with different colors represent the fraction of χ in the DM component. The Yukawa coupling y_{sf} is constrained within $[2 \times 10^{-8}, 2.5 \times 10^{-6}]$ while m_χ can take value among the chosen parameter space with $[500\text{ GeV}, 3\text{ TeV}]$ under DM relic density constrained. For the fixed m_χ , the larger y_{sf} will contribute to a larger cross section of $h_2h_2 \rightarrow \chi\chi$ so that the fraction of χ will be larger. Particularly, as $y_{sf} > 10^{-6}$, χ production is dominant among DM component. According to Fig. 8(b), we show the viable parameter space of $m_S - \lambda_{dh}$, where points with different colors represent the fraction of S . We have a similar conclusion for the allowed value of m_S and λ_{dh} with case i, where S production is determined by $h_2 \rightarrow SS$ as well as $XX \rightarrow SS$ with X being SM particles. For λ_{ds} , as we can see in Fig. reffig8(c), the

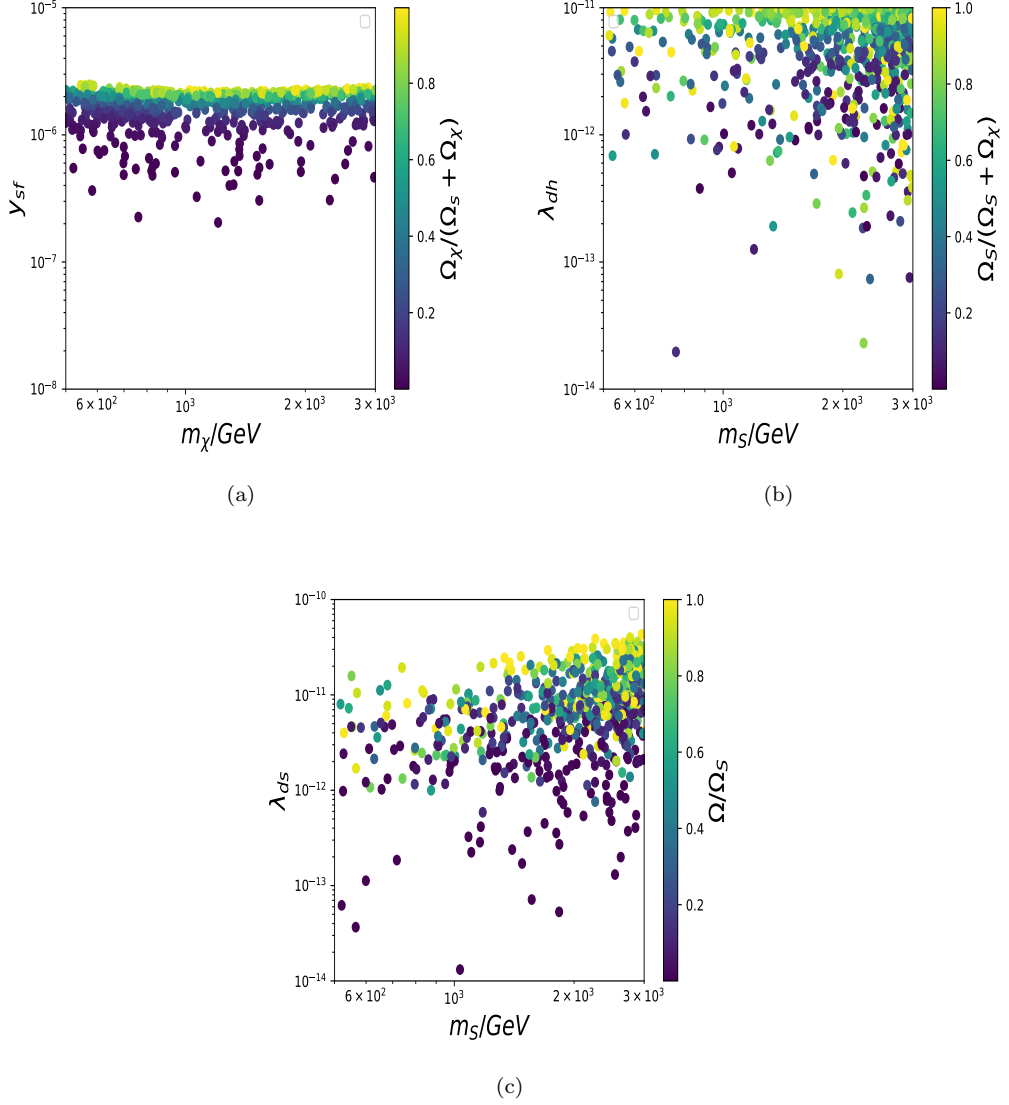


FIG. 9: Same as Fig. 6 but $500\text{GeV} < m_\chi < 3 \text{ TeV}$ and $500\text{GeV} < m_S < 3 \text{ TeV}$.

allowed value for λ_{ds} is $(10^{-21}, 10^{-16})$, where points with different colors correspond to the contribution of h_2 to S relic density. It is obvious that for the larger λ_{ds} , contribution of h_2 to S production is larger and for $\lambda_{ds} > 3 \times 10^{-18}$, S relic density is almost determined by the decay process $h_2 \rightarrow SS$ regardless of the contribution of SM particles.

We give the results of case iv in Fig. 9 with $500\text{GeV} < m_\chi < 3 \text{ TeV}$ and $500\text{GeV} < m_S < 3 \text{ TeV}$, where both S and χ production are obtained via the $2 \rightarrow 2$ annihilation processes. According to Fig. 9, the allowed value for y_{sf} is constrained within $[2 \times 10^{-7}, 2.5 \times 10^{-6}]$ and m_χ can take value among the whole chosen parameter space with $500\text{GeV} < m_\chi < 3 \text{ TeV}$, where points with different colors represent the fraction $\Omega_\chi/(\Omega_\chi + \Omega_S)$. Similar to case iii, a larger y_{sf} will always contribute to a larger fraction of χ in the DM component. In Fig. 9(b), we show the viable parameter space of $m_S - \lambda_{dh}$ under DM relic density constraint, where λ_{dh} is limited within $[10^{-14}, 10^{-11}]$ and m_S can take value among the chosen mass region with $[500 \text{ GeV}, 3 \text{ TeV}]$. For the larger m_S , the allowed value for λ_{dh} is more flexible. On the other hand, for the larger λ_{dh} , the fraction of S is larger. Particularly, as $\lambda_{dh} \approx 10^{-11}$, DM component is mainly constituted by the S production. In Fig. 9(c), we give the viable parameter space of $m_S - \lambda_{ds}$, where points with different colors correspond to the contribution of h_2 to S production, and here Ω is determined by the process of $h_2 h_2 \rightarrow SS$. As we can in Fig. 9(c), λ_{ds} is limited within about $[10^{-14}, 5 \times 10^{-11}]$ under DM relic density constraint. For $\lambda_{ds} < 10^{-12}$, the fraction Ω/Ω_S is much small and SM particles play a dominant role in determining S production. With the increase of λ_{ds} , the fraction Ω/Ω_S increases due to the large annihilation cross

section. Particularly, as $\lambda_{ds} > 2 \times 10^{-11}$ and $m_S > 1$ TeV, the fraction Ω/Ω_S is approximately 1 and S relic density is almost determined by the process $h_2 h_2 \rightarrow SS$ regardless of the contribution of the SM particles.

As a summary, both m_S and m_χ can take values ranging from [1 GeV, 3 TeV] under the DM relic density constraint. On the other hand, contribution of different processes to DM production are different, which depend on the mass hierarchies between DM particles and h_2 , and the allowed values for the couplings can therefore be different. In the case of $m_\chi < m_2/2$, χ production is obtained via the decay process $\chi \rightarrow h_2 h_2$, and for $m_\chi > m_2/2$, the process $h_2 h_2 \rightarrow \chi \chi$ will contribute to χ relic density. For the above two mass regions, the allowed value for y_{sf} are completely different. On the other hand, for the coupling λ_{dh} , we have a flexible parameter space since one can always fine-tune other free parameters to obtain the correct DM relic density. However, for λ_{ds} , we will have four different allowed parameter spaces for the four different cases, since processes related to h_2 can be related to v_0 , which is equal to m_χ/y_{sf} , and a tiny y_{sf} will always induce a much large v_0 so that a large cross section, and the allowed value for λ_{ds} is therefore more constrained, where λ_{ds} can be as small as 10^{-20} level. However, S production can still be almost determined by the h_2 related processes for the tiny λ_{ds} regardless of the contribution of SM particles.

V. SUMMARY AND OUTLOOK

We studied the FIMPs scenario in a two-component dark matter model under $Z_2 \times Z_4$ symmetry, where S and χ are dark matter candidates carrying $Z_2 \times Z_4$ charge. We also introduce a singlet scalar S_0 with non-zero vev so that χ can obtain mass after SSB. For the FIMPs scenario, χ and S production are generated individually in the case of decoupling limit, where we have six parameters with three masses and three dimensionless parameters. Depending on the mass hierarchy between dark matter and half of the new Higgs mass, the contribution of different channels to DM relic density will be different, so that we will have different viable parameter spaces. We therefore consider the four possible cases and studied the relic density as a function of the parameters of the model and determined the regions of parameter space that are consistent with the observed dark matter abundance. Our results demonstrate that the FIMPs scenario is viable over a wide range of masses and couplings, where the coupling λ_{ds} can be as tiny as $\mathcal{O}(10^{-20})$ level, and the new Higgs can play a dominant role in determining DM production.

Appendix A: Appendix

1. Formulas

The expression of the cross section of $h_2 h_2 \rightarrow SS$ is given as follows:

$$\sigma_{h_2 h_2 \rightarrow SS} = \frac{\lambda_{ds}^2}{8\pi s(s-4m_2^2)} \left(\frac{\sqrt{(s-4m_2^2)(s-4m_S^2)} \left(\frac{8\lambda_{ds}^2 m_\chi^4}{m_2^4 - 4m_2^2 m_S^2 + m_S^2 s} + \frac{y_{sf}^4 ((s-m_2^2) + 3m_2^2)^2}{(m_2^2 - s)^2} \right)}{y_{sf}^4} \right. \\ \left. + \frac{8\lambda_{ds} m_\chi^2 \log \left(\frac{-\sqrt{(s-4m_2^2)(s-4m_S^2)} - 2m_2^2 + s}{\sqrt{(s-4m_2^2)(s-4m_S^2)} - 2m_2^2 + s} \right) \left(\frac{m_\chi^2 \left(\frac{3m_2^2 y_{sf}^2}{m_\chi^2 (s-m_2^2)} - \frac{2\lambda_{ds}}{s-2m_2^2} \right)}{y_{sf}^2} + 1 \right)}{y_{sf}^2} \right) \quad (A1)$$

According to Eq. A1, for the process $h_2 h_2 \rightarrow SS$, the cross section will increase with the increase of λ_{ds} but decrease with the increase of m_2 . Note that a larger m_χ and smaller y_{sf} will contribute to a larger cross section, though χ makes little difference in S relic density, and what matters is v_0 defined by the ratio of m_χ/y_{sf} . In the case of "Freeze-in" mechanism, y_{sf} is tiny and the ratio m_χ/y_{sf} will be much larger so that the value of λ_{ds} should be much smaller under the DM relic density constraint compared with the traditional FIMP models.

2. Evolution of Boltzmann equations

In Fig. 10, we show the evolution of dark matter abundance Y_S (left) and Y_χ (right) with the temperature T . We have fixed $y_{sf} = 10^{-9}$, $\lambda_{ds} = 10^{-14}$, $\lambda_{dh} = 10^{-11}$ and $m_2 = 1$ TeV. In Fig. 10(a), we fix $m_\chi = 100$ GeV, and the colored lines correspond to the results of $m_S = 40$ GeV, $m_S = 300$ GeV, $m_S = 800$ GeV, and $m_S = 1200$ GeV, respectively. S production is obtained via the "Freeze-in" mechanism, and in the early universe, the density of S can be negligible. With the decrease in temperature, S relic density is obtained via the feeble interactions. For $m_S = 40$ GeV, S production is mainly generated via the decays of h_1 as well as h_2 , the curve corresponding to $m_S = 40$ GeV

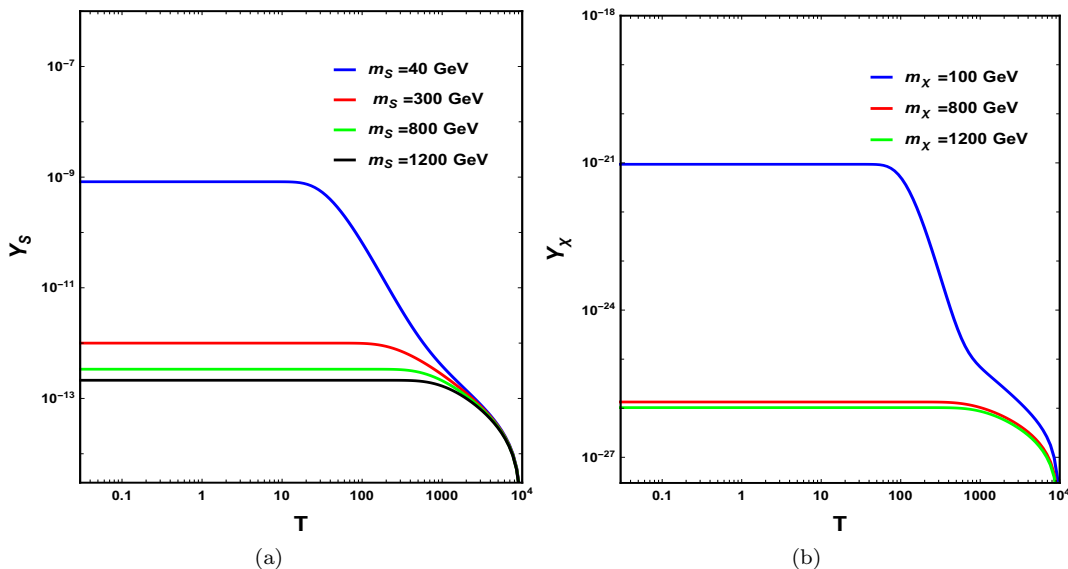


FIG. 10: Evolution of dark matter abundance Y_S (left) and Y_X (right) with the temperature T , where we have fixed $y_{sf} = 10^{-9}$, $\lambda_{ds} = 10^{-14}$, $\lambda_{dh} = 10^{-11}$ and $m_2 = 1$ TeV. In Fig. 10(a), we fix $m_\chi = 100$ GeV, and the colored lines correspond to the results of $m_S = 40$ GeV, $m_S = 300$ GeV, $m_S = 800$ GeV and $m_S = 1200$ GeV respectively. In Fig. 10(b), we fix $m_S = 1200$ GeV and vary m_χ with $m_\chi = 100$ GeV, $m_\chi = 800$ GeV and $m_\chi = 1200$ GeV.

is therefore above other curves for the fixed couplings. According to Fig. 10(b), we fix $m_S = 1200$ GeV and vary m_χ with $m_\chi = 100$ GeV, $m_\chi = 800$ GeV and $m_\chi = 1200$ GeV, while other parameters are unchanged as Fig. 10(a). Similarly, for $m_\chi = 100$ GeV, χ production is mainly determined by the decay process of $h_2 \rightarrow \chi\chi$, and the curve representing $m_\chi = 100$ GeV is therefore above other curves for the fixed couplings.

Acknowledgments

Hao Sun is supported by the National Natural Science Foundation of China (Grant No.12075043, No.12147205). XinXin Qi is supported by the National Natural Science Foundation of China (Grant No.12447162).

[1] N. Aghanim et al. (Planck), *Astron. Astrophys.* **641**, A6 (2020), 1807.06209.
[2] N. Bernal, M. Heikinheimo, T. Tenkanen, K. Tuominen, and V. Vaskonen, *Int. J. Mod. Phys. A* **32**, 1730023 (2017), 1706.07442.
[3] L. J. Hall, K. Jedamzik, J. March-Russell, and S. M. West, *JHEP* **03**, 080 (2010), 0911.1120.
[4] C. Boehm, P. Fayet, and J. Silk, *Phys. Rev. D* **69**, 101302 (2004), hep-ph/0311143.
[5] V. Barger, P. Langacker, M. McCaskey, M. Ramsey-Musolf, and G. Shaughnessy, *Phys. Rev. D* **79**, 015018 (2009), 0811.0393.
[6] K. M. Zurek, *Phys. Rev. D* **79**, 115002 (2009), 0811.4429.
[7] S. Profumo, K. Sigurdson, and L. Ubaldi, *JCAP* **12**, 016 (2009), 0907.4374.
[8] Z.-P. Liu, Y.-L. Wu, and Y.-F. Zhou, *Eur. Phys. J. C* **71**, 1749 (2011), 1101.4148.
[9] X. Qi and H. Sun, *Chin. Phys.* **49**, 103101 (2025), 2411.11236.
[10] M. Pandey, D. Majumdar, and K. P. Modak, *JCAP* **06**, 023 (2018), 1709.05955.
[11] S. Bhattacharya, P. Poulose, and P. Ghosh, *JCAP* **04**, 043 (2017), 1607.08461.
[12] S. Bhattacharya, P. Ghosh, T. N. Maity, and T. S. Ray, *JHEP* **10**, 088 (2017), 1706.04699.
[13] S. Bhattacharya, P. Ghosh, J. Lahiri, and B. Mukhopadhyaya, *Phys. Rev. D* **108**, L111703 (2023), 2211.10749.
[14] A. S. Sakharov and M. Y. Khlopov, *Phys. Atom. Nucl.* **57**, 651 (1994).
[15] M. Khlopov, *Prog. Part. Nucl. Phys.* **116**, 103824 (2021).
[16] B. Díaz Sáez, P. Escalona, S. Norero, and A. R. Zerwekh, *JHEP* **10**, 233 (2021), 2105.04255.
[17] B. Díaz Sáez and P. E. Contreras, *JCAP* **03**, 010 (2024), 2307.07760.
[18] G. Bélanger, A. Pukhov, C. E. Yaguna, and O. Zapata, *JHEP* **09**, 030 (2020), 2006.14922.

- [19] G. Bélanger, A. Pukhov, C. E. Yaguna, and O. Zapata, JHEP **03**, 100 (2023), 2212.07488.
- [20] X. Qi and H. Sun, JCAP **08**, 002 (2025), 2504.12876.
- [21] P. Borah, P. Ghosh, and A. K. Saha, JCAP **05**, 035 (2025), 2412.17141.
- [22] X. Qi and H. Sun (2025), 2510.04610.
- [23] S. Esch, M. Klasen, and C. E. Yaguna, JHEP **09**, 108 (2014), 1406.0617.
- [24] C. E. Yaguna and O. Zapata, Phys. Rev. D **105**, 095026 (2022), 2112.07020.
- [25] C. E. Yaguna and O. Zapata, Phys. Rev. D **109**, 015002 (2024), 2308.05249.
- [26] S. Bhattacharya, P. Ghosh, and N. Sahu, JHEP **02**, 059 (2019), 1809.07474.
- [27] T. Blazek, P. Matak, J. Ramaj, and M. Sabova, Eur. Phys. J. C **85**, 801 (2025), 2504.15164.
- [28] D. López-Val and T. Robens, Phys. Rev. D **90**, 114018 (2014), 1406.1043.
- [29] T. Robens, in 55th Rencontres de Moriond on QCD and High Energy Interactions (2021), 2105.07719.
- [30] V. Khachatryan et al. (CMS), JHEP **10**, 144 (2015), 1504.00936.
- [31] M. J. Strassler and K. M. Zurek, Phys. Lett. B **661**, 263 (2008), hep-ph/0605193.
- [32] J.-J. Zhang, Z.-L. Han, A. Liu, and F.-L. Shao, Nucl. Phys. B **1014**, 116864 (2025), 2411.06744.